DRAG MEASUREMENTS ACROSS PATTERNED SURFACES IN A LOW REYNOLDS NUMBER COUETTE FLOW FACILITY

by

TYLER JAY JOHNSON

A THESIS

Submitted in partial fulfillment of the requirements
for the degree of Master of Science in the
Department of Aerospace Engineering
in the Graduate School of
The University of Alabama

TUSCALOOSA, ALABAMA

2009

Copyright Tyler Jay Johnson 2009
ALL RIGHTS RESERVED

ABSTRACT

Understanding fluid dynamic drag, and its reduction, has always been a topic of primary concern. Direct drag measurements can be difficult to obtain with low viscosity fluids such as air or water. For this study a new low Reynolds number Couette facility was constructed to investigate surface drag. In this facility, mineral oil was used as the working fluid to increase the shear stress across the surface of the experimental models. A mounted conveyor creates a flow within a Plexiglas tank. The experimental model of a flat or patterned surface was suspended above the moving belt. The experimental plate was attached to linear bearings on a slide system that connects to a force gauge used to measure the drag. Within the gap between the model and moving belt a Couette flow with a linear velocity profile was created. Digital particle image velocimetry was used to confirm the velocity profile.

A patterned surface, in this case consisting of 2-D cavities, was embedded into a large portion of a Plexiglas plate. First, the drag across a flat plate of the same size was measured and compared to theoretical values for laminar Couette flow. These results were found to be within 5% of predicted values following $C_D = 2/Re$. The drag for a 2-D embedded square cavity model was then measured and compared to the flat plate results. A drag reduction of up to 20% was found for the lateral rib model at Re ~ 10 or less, with increasing drag reduction as the Re decreases. Lower drag reduction was found up to Re ~ 50, where the difference becomes negligible. Finally, the flow over the 2-D cavities was modeled with a partial slip at the bottom

wall. Modeled average partial slip velocities were calculated from the drag measurements and reached values of 10-22% of the belt speed for $Re < 10$.

LIST OF ABBREVIATIONS AND SYMBOLS

A	Surface area of experimental model
β	Non-dimensional gap height over cavity width
C_f	Coefficient of friction
d	Cavity depth
F	Drag force
γ	Specific gravity
h	Channel half-height
l	Cavity width
μ	Dynamic viscosity
ρ	Density
Q	Volumetric flow rate
Re	Reynolds number based on channel height
τ	Surface shear stress
U_b	Belt velocity

u_s	Partial slip velocity
$\bar{v}$	Average velocity
w	Channel width
y	Location from channel centerline

ACKNOWLEDGEMENTS

I would like to thank Dr. Amy Lang for giving me the opportunity to work in her lab and continue my graduate work at the University of Alabama. Thanks for her guidance and help in accomplishing all the goals of my research work. I would also like to thank my committee members Dr. L Michael Freeman and Dr. John Baker.

I would also like to thank all of the guys in the engineering machine shop especially Tim Connell and Jim Edmonds. Without their help I never could have finished this research. I also want to thank my parents for their support and encouragement with my education through these years. Thanks also to Nikki Wheelus for her help with the PIV measurements.

CONTENTS

ABSTRACT..... ...ii

LIST OF ABBREVIATIONS AND SYMBOLS..... ...iv

ACKNOWLEDGEMENTS..... ...vi

LIST OF TABLES..... ...x

LIST OF FIGURES..... ...xi

1. INTRODUCTION..... ...1

    1.1 Drag Reduction and Couette Flow..... ...1

    1.2 Objectives..... ...2

2. REVIEW OF LITERATURE..... ...5

    2.1 Previous Oil Facilities..... ...5

    2.2 Couette Flow Experiments..... ...6

    2.3 Riblet Drag and Drag Reduction..... ...10

3. THEORETICAL BACKGROUND..... ...15

    3.1 Couette Flow..... ...15

3.2 Reynolds Number and Transition..... ...16

3.3 Drag..... ...17

3.4 Couette Flow Partial Slip Velocities..... ...17

4. EXPERIMENTAL SETUP..... ...20

4.1 Couette Flow Facility..... ...20

4.2 Working Fluid..... ...22

4.3 Force Measurement Apparatus..... ...23

4.3.1 Force Gauge..... ...26

4.3.2 Post-Processing Software..... ...26

4.4 Experimental Models..... ...26

4.5 Time-Resolved Digital Particle Image Velocimetry (TR-DPIV)... ...28

4.6 Experimental Procedure and Driving Parameters..... ...30

5. RESULTS AND DISCUSSION..... ...33

5.1 Flow Visualization..... ...33

5.2 Drag Measurements..... ...35

5.2.1 Flat Plate Model..... ...35

5.2.2 Embedded Cavity Model..... ...40

6. CONCLUSIONS AND FUTURE WORK..... ...44

6.1 Couette Flow Facility..... ...44

6.2 Drag Measurements and Partial Slip Velocities..... ...44

6.3 Future Work..... ...45

7. BIBLIOGRAPHY..... ...47

APPENDIX 1..... ...49

APPENDIX 2: Lateral Rib Model Drag Measurements..... ...50

APPENDIX 3: Drag Coefficient Data..... ...51

LIST OF TABLES

Table 1. Drag forces across embedded cavities (Gatski and Grosch 1985)..... ...13

Table 2. Theoretical and measured drag across a flat plate..... ...39

LIST OF FIGURES

Figure 1. Tillmark and Alfredsson apparatus (Tillmark and Alfredsson 1991)..... ...7

Figure 2. Schematic of Daviaud apparatus (Daviaud et al. 1992)..... ...8

Figure 3. Experimental Setups (Leutheusser 1971)..... ...10

Figure 4. Schematic of Bechert et al. experimental setup (Bechert et al. 1989)..... ...11

Figure 5. Eddie formation within the cavities (Scholle 2006)..... ...12

Figure 6. Shear stress across an embedded square cavity (Gatski and Grosch 1985)..... ...14

Figure 7. Simple Couette flow profile (Wikipedia 2009)..... ...15

Figure 8. Simple 2-D embedded cavity Couette flow..... ...18

Figure 9. Motor, gear reducer, and drive shaft outside of tank..... ...21

Figure 10. Side view schematic of Couette flow facility..... ...22

Figure 11. Side view of force measurement apparatus..... ...25

Figure 12. Dimensions of embedded cavities..... ...27

Figure 13. Experimental model with embedded cavities..... ...28

Figure 14. Schematics of DPIV technique (Dantec Corporation)..... ...30

Figure 15. Side view of tank and experimental setup..... ...31

Figure 16. Backwards flow at end of the channel..... ...34

Figure 17. Vortex at corner of tank..... ...34

Figure 18. Velocity profile of channel with flat plate..... ...35

Figure 19. Drag force vs. time over 100 s..... ...36

Figure 20. Drag force vs. belt speed for flat plate model..... ...37

Figure 21. C_D at given Re for flat plate..... ...38

Figure 22. C_D vs. Re for flat plate..... ...39

Figure 23. C_D vs. Re for both models..... ...40

Figure 24. Re vs. % difference C_D for each β value..... ...41

Figure 25. Re vs. α for embedded cavity model..... ...42

Figure 26. Re vs. u_s for embedded cavity model..... ...42

1. INTRODUCTION

1.1 Drag Reduction and Couette Flow

Drag reduction is an important and often studied area within fluid mechanics. By reducing the drag over an object less power, and therefore fuel, is required to move the object. It has been estimated that a drag reduction of just 1% on an airplane could save $200,000 per year. Across the airline industry this would mean billions of dollars of savings and help curb environmental pollution and dependence on foreign oil.

Surface patterning, such as dimples on a golf ball, is a simple, passive means of drag reduction. In this method, embedded or protruding geometries manipulate the flow and create vortices that either delay transition to turbulent flow or cause an early transition to prevent separation of the boundary layer. In this study embedded geometries were used in a completely laminar flow to examine the surface drag resulting from 2-D embedded cavities within which vortices form that allow the outer flow to "slide" over the geometry.

The primary intent of the work performed was to construct a new facility to measure drag forces across the surface of a plate. Water has a low viscosity and does not create enough force to effectively measure drag. In the water tunnel only velocities and Reynolds stresses can be measured which is an indirect method of measuring the drag of a body. Simple Couette flow is a good model for both a laminar boundary layer flow close to the surface of an object, as well as for a time-averaged turbulent flow within the viscous sub-layer. The increased viscosity of the

oil causes a substantial increase in the force across the surface of the plate making the surface force exerted on the plate by the flow measurable; total forces are on the order of 1 N instead of 1 mN.

The new Couette flow facility provides a way to study the area-averaged surface stress imposed by the flow on the experimental models. The shear driven Couette flow created by the viscosity of the oil has a linear velocity profile along the height of the channel. The stress across the surface of the plate creates a net drag force which can be measured by a force gauge.

In this research, both a flat surface and another consisting of 2-D embedded cavities were positioned in the oil tank above a moving belt. A Couette flow was then created in the channel between the model and the belt. The shear stress across the surface of the plate was measured using a force gauge at different belt velocities and channel heights. Finally, the results were compared to discern whether the formation of embedded vortices in the 2-D cavity model for low Re laminar flow could achieve sub-laminar flat plate shear stress. Previous research by Scholle (2005) shows that rotation of embedded vortices within cavities in laminar flows can reduce skin friction drag by creating a sort of fluid roller bearing within the surface geometry. Gatski and Grosch (1985) also computationally found that surface drag across an embedded cavity was less than that of a flat plate.

1.2 Objectives

The goal of these experiments was to find a means of reducing drag by using embedded geometries. The inspiration of this research stems from the work done in previous experiments. Bechert et al. (1989) built a Couette flow facility and compared drag across longitudinal and lateral ribs. However, the lateral ribs created a smaller gap height than for the longitudinal ribs

and caused flow blockage. The research described in this paper tested lateral ribs embedded within a plate and observed its effect on surface drag. Experiments performed in this new facility can be used to compliment data obtained from the University of Alabama water tunnel as similar geometries can be placed in both facilities and studied.

The first objective of this research was to build a Couette flow facility to experimentally generate a theoretical Couette flow, or a linear velocity profile, between a moving belt and a stationary plate. Variations of similar facilities have produced a true linear velocity profile such as Reichardt (1956) and Leutheusser and Chu (1971). A Time-Resolved Digital Particle Image Velocimetry (TR-DPIV) system was used to measure the velocity profile. A dye could not be used because it would permanently color the oil which is not readily replaceable like water.

Because few facilities of this kind exist, knowledge learned from previous work was limited. Those facilities conducting similar research are much larger, using thousands of gallons of oil or glycerine. This facility would show that research in drag reduction can be done on a smaller scale and with considerably fewer costs.

The second objective of this research is to measure the drag force of a Couette oil flow at various velocities across a flat plate and compare it to the drag force across embedded geometries, specifically for this study across a geometry consisting of 2-D lateral embedded square cavities. The total drag force across the surface of the experimental models can be measured; these measurements were the first of their kind to confirm whether sub-laminar drag is achievable across embedded cavity geometries as has been computationally predicted at low Re by Scholle (2005) and Gatski and Grosch (1985). However, the local types of drag occurring

across the geometry composed of both pressure and skin friction drag, which combined define to total surface drag, could not be differentiated with this measurement technique.

2. REVIEW OF LITERATURE

2.1 Previous Oil Facilities

Very few facilities have been built where high viscosity oil is the working fluid. Those oil facilities that have been constructed are primarily used to study boundary layers and drag reduction. The high viscosity of oil increases the thickness of the boundary layer and size of the viscous length scale as compared to a boundary layer within water or air flow. With this increased thickness, the small scales occurring in boundary layer transition and separation are more easily visualized. The increased kinematic viscosity of oil, combined with a density similar to that of water, causes a much larger shear stress across surfaces within an oil flow. The increased shear forces can be measured with typical force balances and gauges. Different geometries and surface patterning can then be studied within an oil flow for drag reduction research.

Choosing a particular fluid for high viscosity facilities is extremely important and specific for each experiment. In almost all cases the fluid must be safe for human touch and use in laboratory settings. Oil with low flammability is recommended as heat is often added to flowing oil by a motor, pump, impeller, or drive shaft. Using this knowledge the Pennsylvania State University Boundary Layer Research Facility uses glycerine as the working fluid (Bakewell 1966). Glycerine is in use at the facility because of its high viscosity allowing measurements to be taken more easily within the boundary layer. Glycerine also possesses low toxicity making it safe to use in a laboratory and easily obtainable without special permits.

Bechert et al. (1992) working on the Berlin oil channel realized that certain oils have a high sensitivity to light and become dark after exposure to ultraviolet light. Flow visualization via dye or particle image velocimetry (PIV) is not possible with an opaque fluid. Studying drag reduction Bechert et al. also required a fluid that would meet four requirements for the facility: first, produce a thick viscous sublayer that would allow 5 mm for lateral rib spacing; second, create shear stresses greater than 1 N/m^2; third, allow for integration times of a few minutes with flow above 0.5 m/s so that turbulent fluctuations can be accounted for; and finally, support hot wire measurements. White paraffine oil (baby oil) was found to best meet these facility requirements.

Material compatibility is another concern in the use of oil facilities. Esther based oils react with plastics which could change the physical properties of the fluid. Various oil based products also tend to react with rubber products which would contaminate and possibly color the oil. The California Institute of Technology also employs the use of an oil channel for research with small low-aspect ratio wings in low Reynolds flow (Munson 2009). This facility uses Chevron Superla white mineral oil which reacts with some forms of metal as well. Copper and bronze were found to react with this oil and leave it a deep yellow color preventing flow visualization. In these oil facilities, the particular choice of viscous fluid is important on the range of experiments that can be performed and materials that can be used.

2.2 Couette Flow Experiments

Most studies of Couette flow have been performed theoretically by solving the Navier-Stokes equations. Few experiments have actually taken place trying to create the linear velocity and shear stress profile of Couette flow in a laboratory setting. However, many ideas exist as to

how to produce Couette flow. The first method is to loop a belt around two cylinders and immerse the device in a liquid as done by Reichardt (1956). By moving the belt at a constant speed Couette flow was created within the belt from the centerline to the belt. The center had zero velocity as the belt moved in opposite directions on either side. Reichardt searched for the point of transition for Couette flow within his system and determined the critical Reynolds number to be approximately 750. Likewise, Tillmark and Alfredsson (1992) used this same approach as they investigated the transition Reynolds number for plane Couette flow. With this experimental configuration the investigators found it difficult to achieve a linear velocity profile within the channel even for laminar flow. The resulting velocity profile was often an S-curve which could have been a result of turbulence in the system. Through experimentation, Tillmark and Alfredsson found a transition Reynolds number of approximately 360.

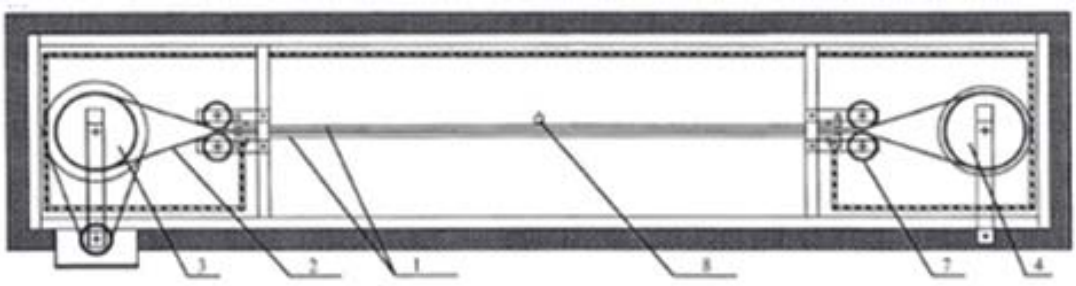

Figure 1. Tillmark and Alfredsson apparatus. (1) floated glass plates, (2) polyester belt, (3) driving cylinder, (4) belt support and speed measuring cylinder, (7) belt steering cylinders, (8) liquid jet injector (Tillmark and Alfredsson 1991).

In almost an identical experimental setup to Tillmark and Alfredsson, Daviaud et al. (1992), found similar results. They concluded the transition Reynolds number to be approximately 370.

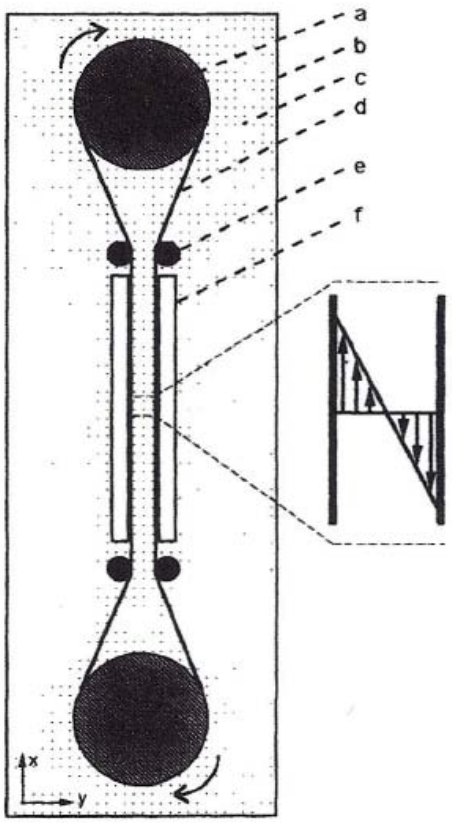

Figure 2. Schematic of Daviaud apparatus. (a) Large cylinders, (b) tank, (c) water, (d) clear plastic belt, (e) small cylinders, and (f) glass plates (Daviaud et al. 1992).

Robertson (1959) used the belt loop but instead placed a stationary plate above the surface of the belt. Focusing on the air flowing between the belt and plate, Robertson was able to get results closer to true Couette flow. The flow was mostly linear except very close to the plate and belt where it had curvature as previously found by Reichardt.

Leutheusser and Chu (1971) found another way to approach Couette flow. A moving water surface was used as the moving surface of a Couette channel while a rigid, plastic-coated piece of plywood was the stationary surface. Air flowing between these surfaces would create the linear velocity profile associated with Couette flow. The water sat upon a tilting laboratory flume which could be used to vary the velocity of the moving surface. This setup could produce accurate results but as the water velocity increased so did the possibility for inaccuracies due to

rippling within the water. For laminar flows, Reynolds numbers (based on center-line velocity and channel half-depth) below approximately 280, linear velocity profiles seemed to exist. As this critical Reynolds number differs from that found by Reichardt, the researchers believed that the transition point varies within each experimental setup.

Aydin and Leutheusser (1979) experimented with Couette flow by moving one rigid Plexiglas plate over another stationary glass plate. The top plate was attached to a mechanical carriage that moved across the stationary plate at a constant velocity causing air, the working fluid, to move between the plates. Since two identical rigid walls were used the effect of wall roughness could be studied with this system. The group was able to replicate a linear velocity profile for laminar flow within the apparatus. For turbulent flow, the S-shaped velocity profile, as discovered by previous researchers, was also found. Experimentally the critical Reynolds number was found to be approximately 280.

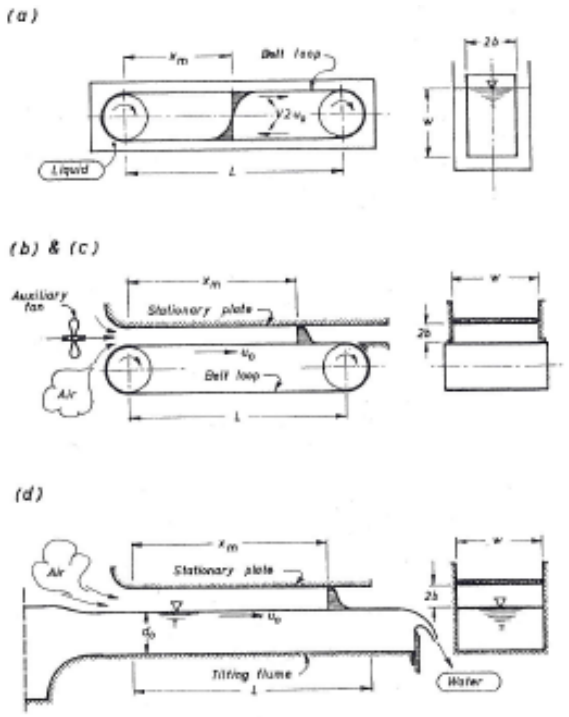

Figure 3. Experimental setups (a) Reichardt apparatus, (b) Reichardt apparatus, (c) Robertson apparatus, (d) Leutheusser and Chu apparatus (Leutheusser 1971).

2.3 Riblet Drag and Drag Reduction

Surface patterning, such as dimples on a golf ball, is one way to reduce drag on an object within a flow. Riblets, one example of surface patterning, have been found to reduce skin friction drag by up to 10% in turbulent flow. The drag reduction in a laminar flow has not been studied extensively.

As a precursor to the Berlin oil channel, Bechert et al. (1989) filled a small tank with glycerine and placed a belt loop inside. A plate with longitudinal ribs was placed above the belt while a plate with ribs aligned laterally to the flow was placed below the belt. These plates were connected to a frame attached to springs so as to measure the shear stress across the surface of

the plates. From these experiments Bechert et al. found that the shear stress was greater across the lateral riblets. Below a diagram of the experimental apparatus is shown.

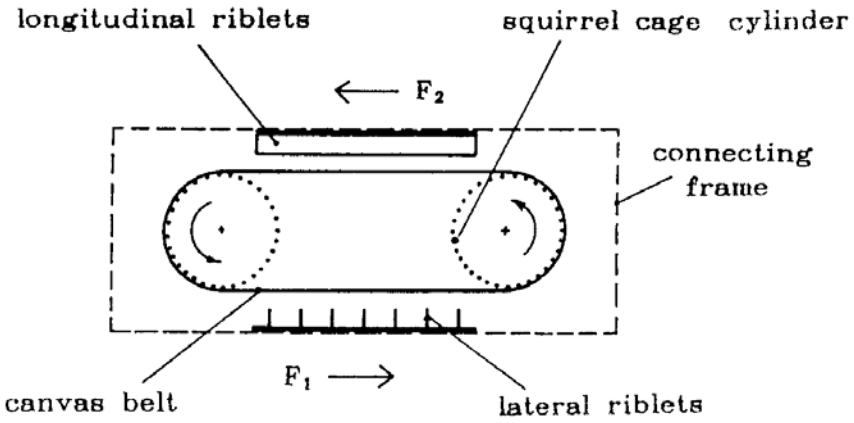

Figure 4. Schematic of Bechert et al. experimental setup (Bechert et al. 1989).

Bechert et al. acknowledged that the decrease in gap height for the lateral ribs caused blockage of the flow and therefore an increased shear stress. Eliminating this difference in gap height and embedding the ribs within a plate should decrease the shear stress which may prove to be equal or below that of longitudinal ribs.

Scholle (2006) computationally examined the effect of a lateral, sinusoidally shaped surface on low Reynolds creeping flows. After equation manipulation and a Fourier analysis, Scholle discovered that the surface pattern with sharper peaks could reduce drag by up to 10% as opposed to riblets with smoother shaped sinusoidal peaks. The reduction is a result of vortices formed within the valley of the peaks that force the moving fluid away from the surface. The vortices and fluid within them create a roller bearing effect reducing the shear stress across the surface. It was found that sharper peaks improve the mean transport velocity which produces a stronger reduction in drag. As can be seen in the figure below, eddies form in the cavities

between the peaks, the inner flow, and push the rest of the flow, the outer flow, away from the surface of the model creating a roller bearing effect.

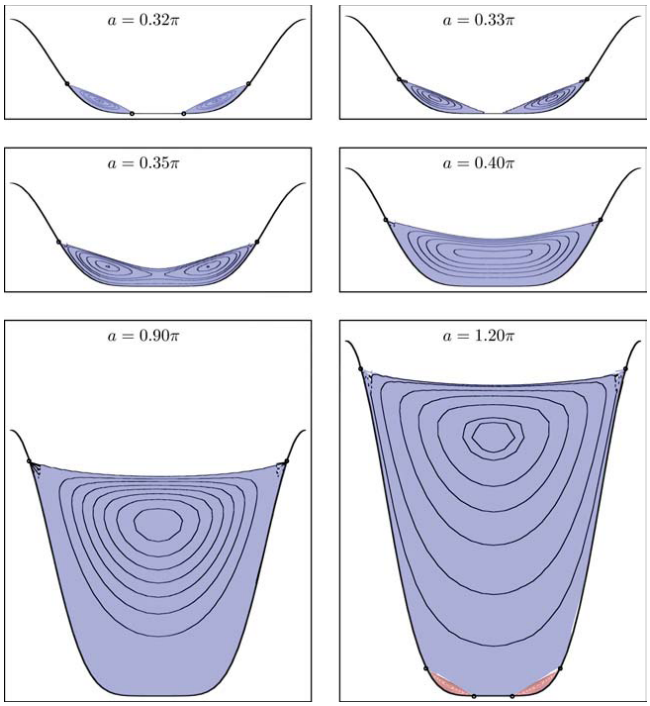

Figure 5. Eddie formation within the cavities (Scholle 2006).

The maximum increase in the mean transport velocity was found to be approximately 1%, which although small could be significant in terms of drag reduction. Wang (1994) analytically studied the drag across a finned plate (like lateral riblets shown in figure 4) in a creeping or Stokes flow, Re << 1. He claimed to have found an increase in drag across the finned plate when compared to a flat plate; this was due to the fact that adding the fins, or cavity partitions, actually resulted in decreasing the gap distance which causes corresponding drag increase. However, using the same reference point as used in this study, flat plate drag value for the plate located at the top of the cavities, the drag actually decreases across the finned plate. Wang also observed a greater decrease in drag for longer than wide cavities. For square cavities

with a gap height the same as the cavity height, they observed a decrease in drag of approximately 20% (see Appendix 1).

Gatski and Grosch (1985) studied the drag across an embedded 2-D cavity in a laminar boundary layer flow. They computationally examined how changing the ratio of the size of a square cavity to the boundary layer thickness affected the drag across the surface of the plate for a Re value of about 1200 based on boundary layer thickness. This research found that the greatest reduction in drag occurred at a cavity length to boundary layer thickness ratio of ¾. At higher ratios, and thus higher cavity Re, the results showed the cavity vortex being pushed towards the downstream side of the cavity with a corresponding decrease in drag reduction. The authors postulated this trend would continue at larger ratios as at the 1:1 ratio the greater reduction in friction drag did not overcome the greater increase in pressure drag from increased cavity size. The table below shows the drag decrease at changing cavity sizes.

Cavity size	Pressure drag ($\times 10^{-4}$)	Differential friction drag[a] ($\times 10^{-4}$)	Total differential drag[b] ($\times 10^{-4}$)	Percent reduction[c]
$\ell = d = 1/4$	1.4	−2.0	−0.6	−0.9
$\ell = d = 1/2$	3.3	−4.2	−0.9	−1.3
$\ell = d = 3/4$	4.9	−6.8	−1.9	−2.4
$\ell = d = 1$	7.5	−8.7	−1.2	−1.5

[a]Frictional drag with cavity minus frictional drag without cavity. [b]Pressure drag plus differential frictional drag. [c]Total differential drag divided by frictional drag on flat plate.

Table 1. Drag forces across embedded cavities (Gatski and Grosch 1985).

Gatski and Grosch (1985) also showed how the shear stress varied linearly across the surface of a plate and an embedded cavity. As seen in the figure below, the shear stress increases at the edges of an embedded cavity but approaches zero over the cavity. The increase ahead of

the cavity is due to a favorable pressure gradient occurring as the flow approaches the cavity upstream.

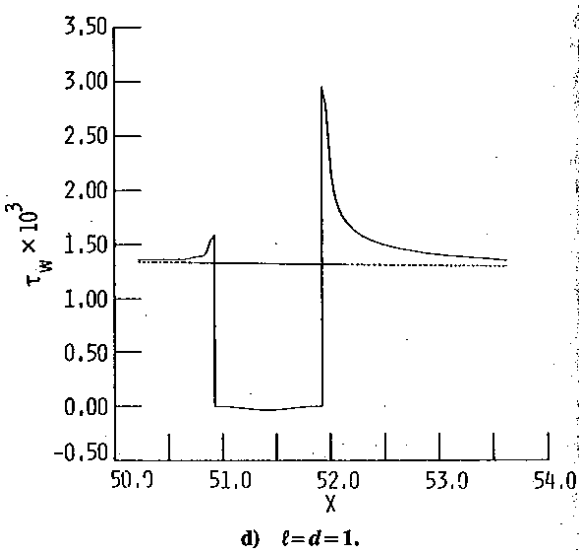

Figure 6. Shear stress across an embedded square cavity (Gatski and Grosch 1985).

3. THEORETICAL BACKGROUND

3.1 Couette Flow

Couette flow is a steady, wall-driven flow that is one of the exact solutions of the Navier-Stokes equations. Couette flow is defined as the laminar flow between two infinite, parallel plates where one plate is moving at a constant velocity *U* and the other plate is fixed. The plates are assumed to be infinite in the z-direction and are separated by a distance of 2*h*, the channel height. Below is a simple Couette flow configuration.

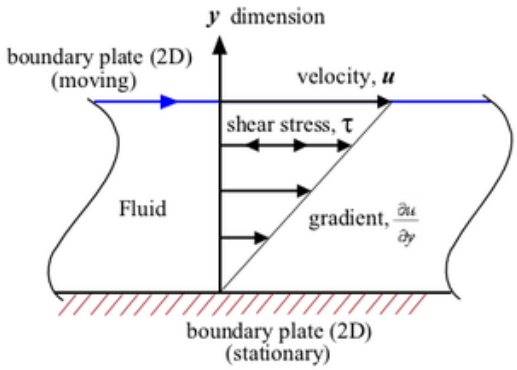

Figure 7. Simple Couette flow profile (Wikipedia 2009).

Viscous drag forces caused by the moving plate drive the flow. The boundary conditions are assumed to be the no slip conditions present at the walls, so $u(+h) = U$ and $u(-h) = 0$. This leads to a linear velocity profile that varies with the channel height. The equation for velocity is shown.

$$u = \frac{U}{2} * \left(1 + \frac{y}{h}\right) \quad (1)$$

Knowing that the dynamic viscosity μ is constant, it can be found that the shear stress is constant and equal to the equation below.

$$\tau = \mu * \frac{du}{dy} = \mu(\frac{U}{2h}) \quad (2)$$

The total drag across the surface of a plate is then equal to:

$$F = \tau * A \quad (3)$$

3.2 Reynolds Number and Transition

The transition from laminar flow to turbulent flow is an important aspect in the study of fluid mechanics. Turbulent flows differ with respect to drag from laminar flows. Laminar flow experiences most of its drag in the form of pressure drag and very little from skin friction drag. The transition from laminar flow to turbulent flow occurs when disturbances in the flow grow uncontrollably and are not dissipated by viscous effects.

One way to determine the transition point of a flow is to determine the Reynolds number. The Reynolds number is a ratio of the inertial forces versus the viscous forces of the flow. The Reynolds number is dimensionless and is defined as $Re = \frac{\rho U 2h}{\mu}$ where *2h* is the characteristic length. For Couette flows the characteristic length is generally chosen to be the gap or channel height. As the Reynolds number increases for a flow, the inertial forces become greater than the viscous forces. When turbulent eddies formed in the flow become amplified and the flow is unable to return to a steady state transition occurs. The critical Reynolds number must be

determined experimentally for each different system as slight differences change the transition point. Experimentally, Aydin and Leutheusser (1979) found the earliest transition point among researchers for planar Couette flow which occurred at a Reynolds number of approximately 280.

3.3 Drag

Drag is the sum of the forces acting parallel to the direction of the flow. Many forms of drag on a body exist such as pressure, induced, skin friction, wave, and interference drag. The most prevalent form of drag over a body in a laminar flow is pressure or form drag. Pressure drag results from the shape of a body moving through a flow. Different shapes result in varying drag forces on an object. The surface drag across embedded geometries will differ and may be lower than the surface drag across a flat plate.

Skin friction drag results from the viscosity of a fluid flowing across the surface of an object, and the only form of drag present in planar Couette flow over a flat plate. A shear stress is created within the boundary layer formed by the fluid. Greater shearing stresses result from fluids with higher viscosities; therefore, higher viscosity fluids create more drag on objects than fluids with low viscosity. This leads to the equation for viscous forces below.

$$dF_v = \tau dA \tag{4}$$

3.4 Couette Flow Partial Slip Velocities

For Couette flow with a flat plate the no slip condition is assumed at the non-accelerating plate surface. However, partial slip velocities occur above embedded cavities in a flow. Even though the flow takes on a zero velocity at the cavity partitions to subsequently accelerate and decelerate after reaching a maximum value over the cavity, an average slip velocity can be

approximated to model the flow over the embedded cavities which results in a decrease in drag. A simple model for 2-D embedded cavity Couette flow is shown in figure 8.

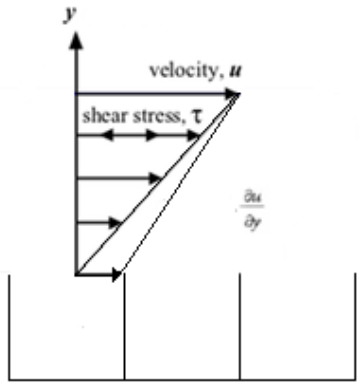

Figure 8. Simple 2-D embedded cavity Couette flow.

The equations for Couette flow can be manipulated in a way similar to that performed by Watanabe et al. (1999) with Poiseuille flow in a pipe. Since the velocity profile is still linear the velocity at any height can be found by the equation below.

$$u = \frac{U_b - u_s}{2h} y + u_s \tag{5}$$

By using the ratio:

$$\frac{u_s}{U_b} = \alpha \tag{6}$$

The velocity equation then reduces to:

$$u = \frac{U_b(1-\alpha)}{2h} y + \alpha U_b \tag{7}$$

Then the equation for volumetric flow rate can be introduced.

$$Q = w\int_0^{2h} u dy = \bar{v}A \tag{8}$$

After solving the integral with the velocity equation inserted the average velocity reduces to:

$$\bar{v} = \frac{U_b}{2}(1+\alpha) \tag{9}$$

Now using the equation of the drag coefficient and shear stress

$$C_D = \frac{\tau}{\frac{1}{2}\rho\overline{v^2}} = \frac{\mu\frac{U_b}{2h}}{\frac{1}{2}\rho(U_b)^2} = \frac{2}{Re} \tag{10}$$

where:

$$\frac{du}{dy} = \frac{U_b(1-\alpha)}{2h} \tag{11}$$

The equation can then be reduced to:

$$C_D = \frac{2}{Re}(1-\alpha) \tag{12}$$

From this final equation it can be found that α is a function of the Reynolds number. As the Re increases α becomes smaller. For this research, the slip velocity must be found from the drag measurements and known test model surface area. Also, for α = 0 the friction coefficient results in a predicted behavior of $C_D = 2/Re$ which will be used to evaluate the flat plate results.

4. EXPERIMENTAL SETUP

4.1 Couette Flow Facility

All experiments were performed in the newly constructed Couette flow facility at the University of Alabama; the design and construction of this facility constitutes a major portion of the work performed under this thesis. The tank is 30 inches wide, 49 inches long, and 23 inches deep giving it a capacity of approximately 150 gallons. The tank is held in a steel frame made of 2 inch angle iron with a 3/8" thickness and was filled with high viscosity oil.

To create an oil flow within the tank a Dorner MPB series conveyor was used. The conveyor is 12 inches wide and 24 inches long with a variable speed motor. The belt on the conveyor is a plastic chain so that oil can pass between the cracks of the belt, however presents a solid moving surface when flat. This prevents the belt from slipping caused by oil build up between the rollers and the belt. Chain guides are in place on the bottom of the conveyor to prevent belt sag. The 12 mm drive shaft on the conveyor is attached to an extension by a flexible coupling. The extension runs through a seal in one side of the tank to connect to the gear reducer as the motor and gear reducer are not to be submerged. An MPB series side mount drive package for standard load is used with a 90 degree hollow shaft gear reducer. The motor is a three phase asynchronous motor with a squirrel cage rotor and slip ring rotor distributed with the conveyor by Dorner. As a further description, it is a 60 Hz gear motor capable of 0.25 horsepower at 345 rpm. A Pacesetter Model 2997 adjustable speed drive controls the speed of

the motor and conveyor. This speed controller is mounted on one corner of the tank near the motor.

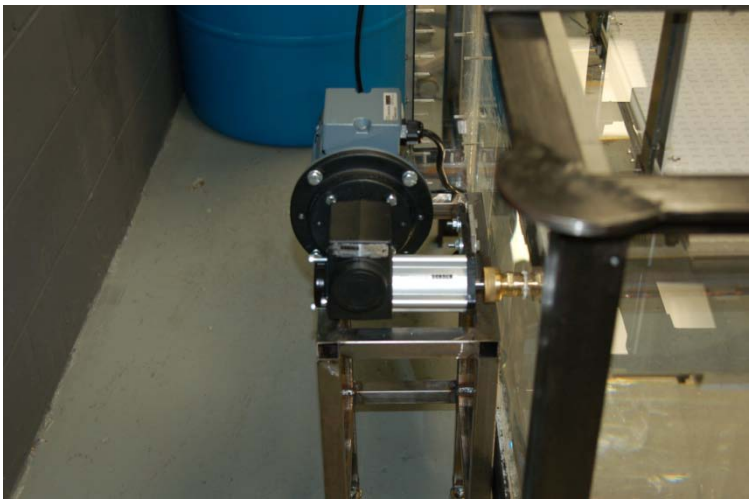

Figure 9. Motor, gear reducer, and drive shaft outside of tank.

The conveyor is suspended in the tank by steel bars attached to mounting plates on the side of the conveyor. The bars are L-shaped and bolted to the steel frame holding the tank. The bars are reinforced by 1 inch square hollow steel rods. This increases the rigidity of the suspended structure and reduces the wobble and vibration caused by the moving conveyor. The conveyor is located 5 inches from the side of the tank near the motor, 11 inches from the front of the tank, and 12 inches from the top of the tank. This setup is removable as well so that the tank can be used for other purposes if necessary.

The velocities were determined by marking a place on the belt and recording a video of the belt for approximately one minute at each mark on the speed controller. Multiplying the distance traveled by the belt by the number of revolutions and dividing that by the time gave an average belt velocity. The conveyor was turned off and on twice and three videos at each speed were analyzed to ensure constant belt speed.

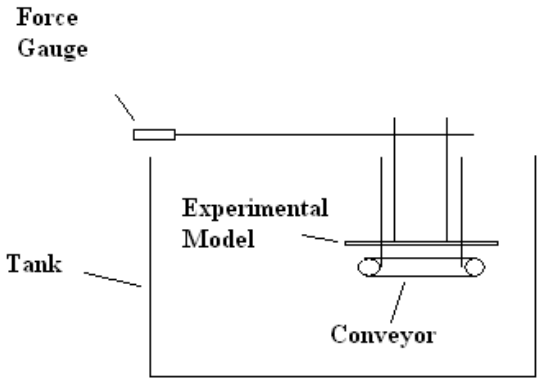

Figure 10. Side view schematic of Couette flow facility.

4.2 Working Fluid

The fluid chosen for this facility must meet many requirements. The fluid needs to have a high viscosity to increase the shear stress, and therefore the total drag force, across the surface of the plate. The preferred viscosity range was on the order of 50-250 centiPoise. The fluid needed to be transparent so that PIV measurements could be taken to determine the velocity of the flow within the tank. The fluid must not vaporize at ambient temperatures. The fluid must also be safe for laboratory use. This means that the fluid is not carcinogenic, has little to no flammability, and is safe for skin contact.

Oil was found to best suit these requirements. However, material compatibility is a concern with most oils. Many oils, particularly ester based oils, react with plastics, which could cause a change in the properties of the oil like viscosity. Almost all oils react with rubber and cause it to break down over time. Many oils also have sensitivity to light and eventually change colors, often becoming black, after long exposures to light. Also, some metals such as copper and bronze tend to react with oil and cause it to take on an orange or yellowish color.

After addressing these concerns, Crystal Plus Oil 500T processed and sold by STE Oil Company, Inc. was chosen for the University of Alabama Couette flow facility. This oil is allowed for food contact by the United States Department of Agriculture so it is safe for human contact and even incidental ingestion. The oil is classified as only slightly combustible by the Occupational Safety and Health Administration. Unlike many oils the Crystal Plus oils possess a low reactivity. This oil is not light sensitive and is only reactive with rubber. According to the manufacturer the oil has $\gamma = 0.86$. Therefore, $\rho = 857.9$ kg/m^3 at the lab temperature of 22.6°C.

The oil is stored in the original 55 gallon barrels in which they arrived. It is pumped to the tank by a close-coupled external gear pump. The pump uses 3/8 inch inside diameter vacuum-rated nylon tubing to pump oil to and from the tank at approximately 1 gallon per minute. When the facility is not in use, the tank is covered by a plastic sheet to prevent dust, bugs, hair, and any other foreign particles from mixing into the oil.

4.3 Force Measurement Apparatus

The force measurement apparatus for this facility measures the total drag across the surface of the experimental model. Pressure drag, form drag, etc. could not be differentiated with this setup. Through previous research and established principles it can be theorized why one model experiences less drag, but in this facility pressure and form drag are combined to measure total surface drag for non-planar geometries.

The force measurement apparatus begins with the experimental model. Four small 2 inch long pieces of ½ inch Plexiglas are glued near each corner at the top of the experimental model. A screw is then placed through each piece attaching the model to a thin aluminum bar to hold the model in place above the conveyor. The aluminum bars are approximately 1 foot long and rise

out of the oil to the top of the tank. Each bar is attached to a 2 inch aluminum angle at the top. The horizontal part of each angle is then screwed together with thin aluminum sheet to one of four linear bearings. The linear bearings have a ½ inch inner diameter and are placed on two ½ inch polished steel rods that run parallel to the length of the conveyor. Each rod has 2 linear bearings on it. The rods run above each side of the conveyor. The thin aluminum sheet keeps the bearings set the same distance apart from one another as the Plexiglas pieces on top of the experimental model. The rods are two feet in length and are supported on each end by a base mount. The base mounts have been secured to steel bars bolted to the steel frame of the tank. These bars give rigidity to the apparatus so that when the facility is in use the model is only moving because of the drag created by the flow. The minimal vibration of the tank caused by the motor and conveyor do not cause the bearings to move on the rods.

The inside of the bearings have small rolling balls in order to reduce the friction between the rods and bearings. In addition to this the rods have been polished further reducing friction. Creating as little friction as possible is necessary for this experiment since the forces are on the order of 1 Newton. Every effort was made to keep the rods as close to parallel as possible so that the bearings do not converge or diverge as they move along the rods preventing movement. To allow for possible deviations that may be present the screws securing the base mounts to the steel bars are not fully tightened. Also, the rods are not tightly secured in the base mounts allowing for slight lateral movements, on the order of a few thousandths of an inch, by the bearings along the path of the rods. To prevent flow from entering the channel downstream of the beginning of the belt, Plexiglas shields were attached to the steel bars on the side of the conveyor.

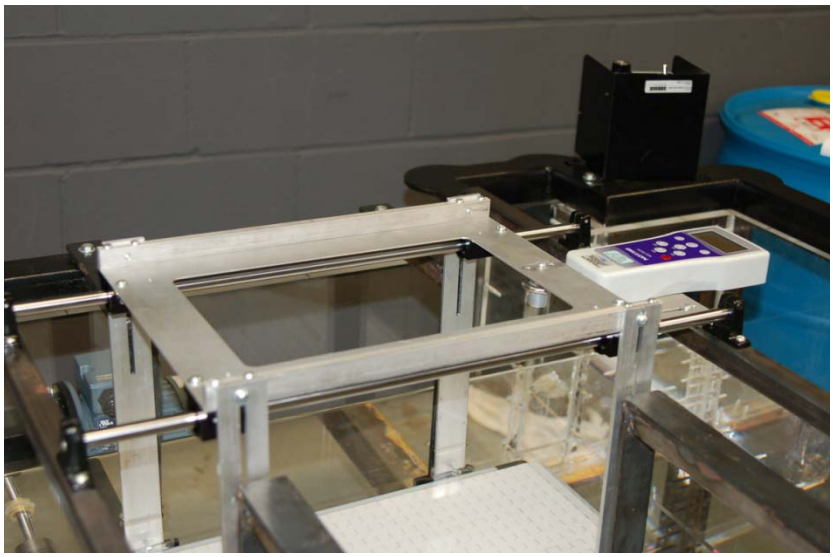

Figure 11. Side view of force measurement apparatus.

To measure the force created by the flow against the surface of the model a pin is attached vertically downward through the aluminum sheet. The force gauge is mounted on an aluminum plate attached to the steel bars holding the plate apparatus. A small 1 inch diameter hook is screwed into the force gauge and can be pushed or pulled to measure force. The pin is placed through the hook so that as the plate is moved by the flow the pin pulls against the hook causing a force to be measured by the gauge.

To account for possible friction between the bearings and the steel rods calibration masses were attached to the apparatus and force measurements were recorded. It was found that for masses up to 200 g, approximately 2 N of force, friction accounted for a difference of less than 5%. For forces greater than approximately 2 N, friction was non-existent in the force measurements recorded by the gauge.

4.3.1 Force Gauge

The force gauge is a Dillon GTX 5 model. This gauge has a 5 Newton capacity with an accuracy of ±0.005 N. The gauge was tested before and after the experiments using a set of calibration weights to ensure accuracy. Known masses of 10 g, 100 g, 200 g, and 500 g were attached to the force gauge and the readings were within the given accuracy of ±0.005 N. For these experiments, the maximum sampling rate of 10 Hz was used. The measurements were sent to the computer using the RS-232 serial cable offered by Dillon. The recordings can also be sent to Microsoft Excel for analysis.

4.3.2 Post-Processing Software

The Dillon Q-Graph 1.5 software was used to analyze the data obtained from the experiments. The software plots the data as either force vs. time or force vs. displacement. The software also automatically gives the minimum, maximum, and average force for the length of the experiment. Using the data from Excel the force plots from different experiments can be placed on a single graph for comparison and analysis of drag across test surfaces.

4.4 Experimental Models

The goal of these experiments was to study the total drag force across the surface of flat plates and plates with embedded geometries. The first experiment was performed with just a flat ½ inch thick Plexiglas plate. The plate is 66 cm (26 in) long and 30.5 cm (12 in) wide. The plate stretches past the edges of the conveyor so that flow hitting the square end of the plate and causing additional drag is not measured. The flat plate was first used as a control study to determine the forces measured over the plate are consistent with theoretically predicted values; any deviation from this value should be due to edge effects. Also, PIV measurements were taken

to ensure the formation of the linear velocity profile and transition to turbulence can be observed if a sufficient Reynolds number is reached. The results of the flat plate experiment can be compared to those done with embedded geometries to see which configuration experiences lower drag forces.

The second set of experiments used an experimental model with embedded lateral ribs. The model consists of a Plexiglas plate with 45 cavities embedded in the center of the plate. The cavities are approximately 0.953 cm (3/8 in) deep, 0.953 cm wide and 25.4 cm (10.0 in) long. The wall or rib between the cavities is approximately 1 mm (40/1000 in) or about 1/10 of the cavity depth. The total area of the plate with embedded cavities was approximately 1202 cm^2 or 59.7 % of the total area. The placement and number of cavities was determined by the location of established Couette flow with minimal side effects over the belt. The cavities were cut out of a ½ inch thick piece of Plexiglas by a precise milling machine which created a round 0.318 cm (1/8 in) fillet at the end of each cavity. Although the cavity is not perfectly square the effect should be minimal and occur only at the edges of the cavities. The embedded cavities within the model can be seen in the figures below.

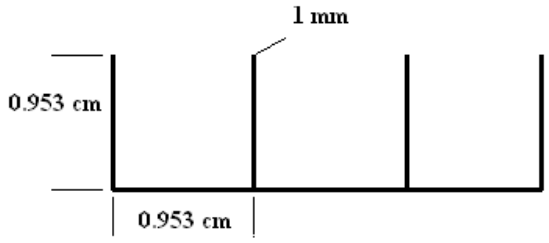

Figure 12. Dimensions of embedded cavities.

Figure 13. Experimental model with embedded cavities.

4.5 Time-Resolved Digital Particle Image Velocimetry (TR-DPIV) System

In order to determine the velocity profile of the region between the moving belt and the fixed experimental model, a digital particle image velocimetry (DPIV) system was used. This technique of flow measurement is non-intrusive. The system uses a laser sheet to illuminate a random group of seeding particles in the flow and auto-correlates the particle displacement between two images where the time difference is known.

The following is a brief description of the DPIV system in use at the University of Alabama. A complete, detailed description of this system can be found in the dissertation by Ardana (2008) and the thesis by Melnick (2009). The oil tank was first seeded with particles. These particles must be very small so as not to alter the flow and according to Melling (1997) non-toxic, non-corrosive, non-abrasive, non-volatile, and chemically inert. Because of this, Conduct-o-Fil ® silver coated hollow glass spheres made by Potter Industries, Inc. were used. These have been used for numerous experiments in the University of Alabama water tunnel with good results as well. For this oil tank the same 18 μm size spheres that are used in the water tunnel were used since the density of the oil is similar to that of water. The seeding density must

be carefully monitored because there must be enough particles for the software to track from frame to frame, but there cannot be so many that the scattered light clouds the images from the camera.

The laser sheet must then be fixed across the plane of the area where the measurement is to be taken. The high speed camera must then be focused on the plane of the laser sheet so that the illuminated particles can be seen. The camera frame speed and laser pulse rate must then be matched so that the particles are visible in each image. The camera sends the images to the computer for storage and processing. Each image is divided into smaller interrogation windows, which are approximately 32 x 32 pixels. The software identifies the particles in each window and calculates the average displacement for each particle from one frame to the next. Knowing the time difference between each image the software is able to calculate the velocity across the entire image. From this vector field, vorticity, Reynolds stresses, and streamlines can be found for the experiment as well.

The components of the TR-DPIV system at the University of Alabama consist of: a Quantronix Falcon 30 Nd:YLF high frequency laser; an 8-bit Basler A504k high speed camera; a Dell Precision workstation with two Intel Xeon processors at 3.2 GHz each and 3 GB of RAM memory; and a frame grabber from National Instruments (PCIe-1429) along with an extension board (Ardana 2008). NI LabVIEW software performed the image acquisition and Pixelflow software was used for post processing of the images. The figure below illustrates the DPIV process used in this experiment.

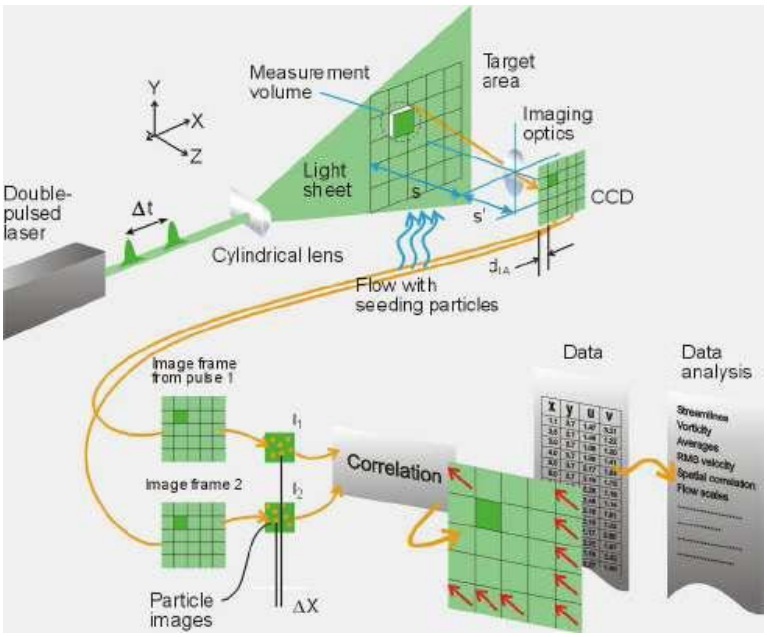

Figure 14. Schematics of DPIV technique (Dantec Corporation).

Using cross-correlation, the technique of finding displacement by comparing consecutive images, Willert and Gharib (1991) found an uncertainty of approximately 1% in translational displacements and 5% in rotational displacements. Because high vorticity regions are related to high velocity regions and this technique uses averages an approximate uncertainty of 10% was calculated for vorticity. These uncertainties are most likely lower for this system since pixel resolution in digital cameras has improved since these numbers were calculated. The improvement of frame grabbers has also decreased these uncertainties.

4.6 Experimental Procedure and Driving Parameters

Accurate placement of the models with respect to the conveyor and to the force measurement apparatus is critical. Shims of equal height are placed on the conveyor near each hanging aluminum bar where the model is screwed together with the bars. The model is placed on the shims and secured in place at the set height of the shims. The shims are then removed

after the model is in place. These steps ensure that the experimental model is not only parallel to the conveyor but also that the surface of the model is at an equidistant height everywhere. This height must be consistent when comparing different surfaces so that the velocity profile is constant. The height can be changed though simply by producing larger or smaller shims.

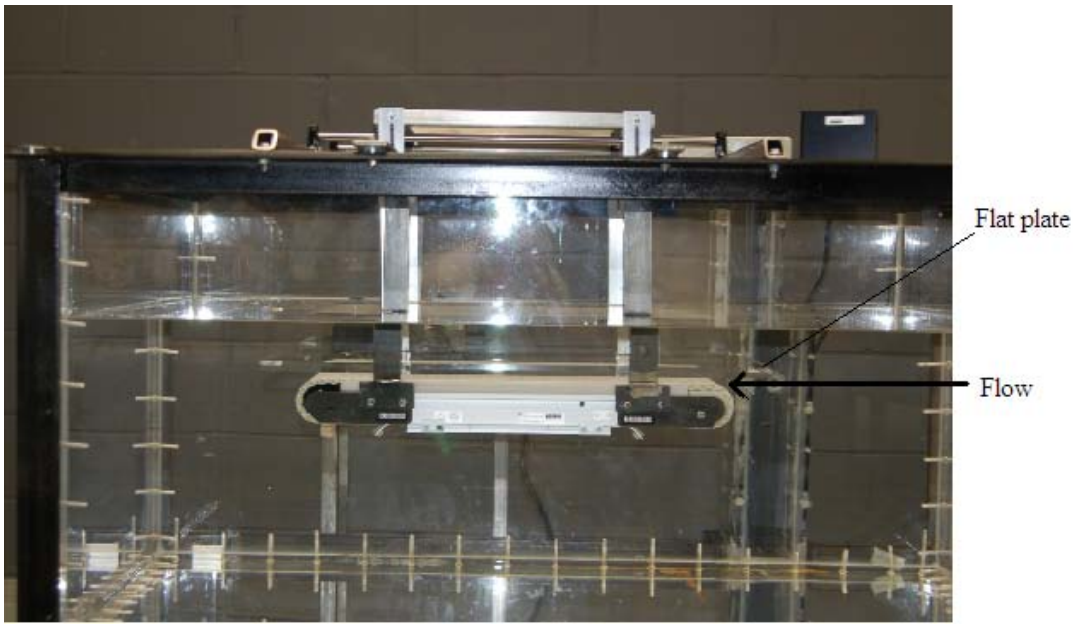

Figure 15. Side view of tank and experimental setup.

The plate must also be positioned correctly over the belt of the conveyor so as to minimize the formation of secondary flows around the plate. With the plate positioned approximately 1.25 inch past the edge of the conveyor where the belt comes up, flow across the top of the plate is almost non-existent. At this position, a stagnation point is created at the edge of the plate and flow in a backwards direction opposite the measured drag is minimized. With the front of the plate, at the left in the figure above, positioned approximately 3/4 inch past the edge of the conveyor, flow being sucked downward by the belt and backward against the surface of the plate is reduced to almost zero.

The velocity of the conveyor must then be chosen for a set of experiments using the speed controller. In order to reduce vibration from the motor and wall effects from the side of the tank, the velocity was kept below the maximum velocity of the conveyor. The Reynolds number for these experiments is based on the center-line velocity and the channel height as specified by previous researchers. The viscosity for the oil is found using a Thermo Fisher Scientific Gilmont falling ball viscometer (GV-2301) with a range of 20-1000 cP. A measurement is taken following each experiment to account for possible heating from the work of the conveyor and drive shaft. Temperature changes were accounted for using a mercury thermometer from Fisher Scientific with accuracy of 0.1°C.

The PIV system was used before the actual drag measurements were taken to make sure the flow was a true Couette flow. The laser sheet was brought in the front wall of the tank to avoid scattering effects caused by sloshing on the surface of the oil. Seeding particles were added slowly to the oil in the tank until enough particles were present in the channel flow for the software to obtain the velocity field at all points in the field of view. For these trial runs, the camera frame rate was set at 500 fps and the laser frequency was 500 Hz. For each trial, 500 image pairs were used for the overall averaging graphs. The PIV analysis could only be used for velocities up to about 38 cm/s because the camera frame rate was limited to 500 fps. Higher belt velocities caused too much particle displacement from frame to frame and an average velocity could not be found by the software. Since the Reynolds number of these experiments is well below the transition point it is reasonable to assume that laminar Couette flow continues at the higher velocities.

5. RESULTS AND DISCUSSION

In this research there were two objectives set forth at the beginning. The first was construction of the new Couette flow facility. After construction the flow through the tank was inspected to ensure that the setup operated as theorized. The secondary flows outside the conveyor belt, above the experimental model, and near the walls of the tank were closely examined to prevent as much interference as possible. The second objective was to measure the drag across embedded cavities and compare it to the drag across a flat plate.

5.1 Flow Visualization

The combination of small bubbles in the tank, caused by air pockets trapped as the oil fills up above the conveyor, and seeding particles illuminated by the laser allowed the flow direction to be seen within the tank. Because of the movement of the belt small vortices were observed to form in the corners of the tank as oil flow hits the walls. As the flow comes up from the bottom where the belt turns to the top side the moving oil hits the plate. At this stagnation point the flow near the belt is swept into the gap between the plate and belt, while the oil outside this point turns away from the gap. At the downstream end of the gap, flow is pulled beneath the conveyor as the belt turns downward creating a slight flow back against the bottom of the plate. This flow is shown as a still shot in figure 15 where the laser illuminates the particles within the flow.

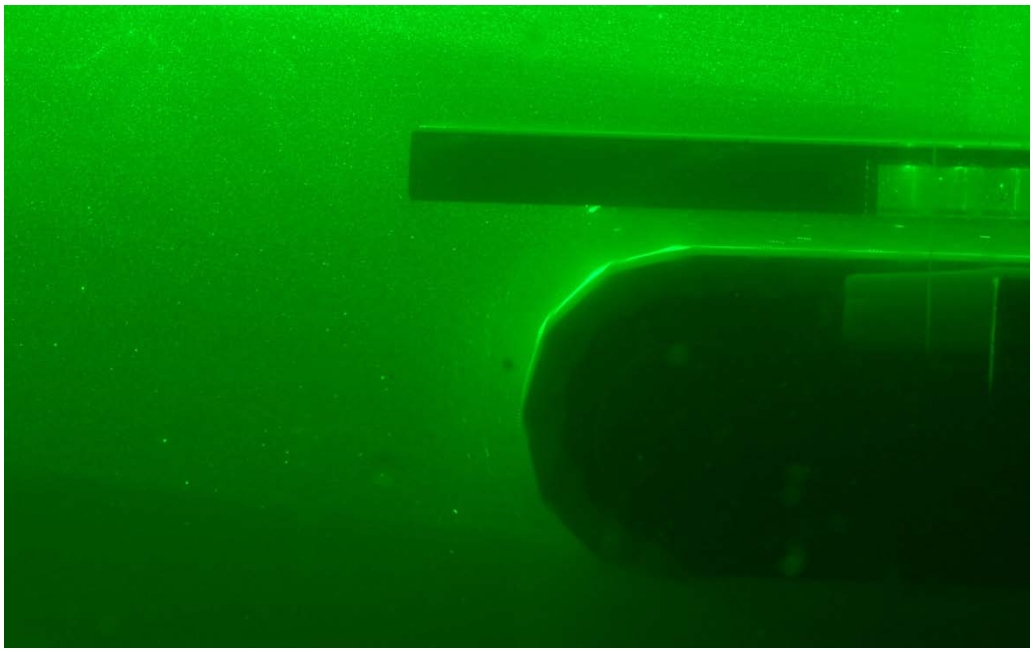

Figure 16. Backwards flow downstream of the gap.

Also, throughout the tank, particularly in the corners, small vortices form and swirl as oil flow hits the walls and is pulled back into the flow created by the moving belt. These secondary flows do not have an effect on the flow within the gap. Although there is a slight flow over the experimental model, it is very slow and located at the surface of the oil away from the model flat plate (i.e. contributes negligible drag to the plate).

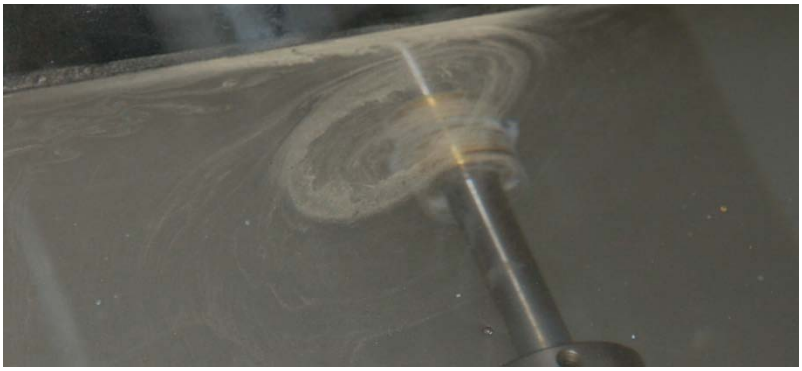

Figure 17. Vortex at corner of tank.

After careful examination of the secondary flows, the DPIV system was used to study the flow within the gap. With the flat plate placed above the conveyor the DPIV system showed that a linear velocity profile was present in the gap thus confirming that a laminar Couette flow was generated between the belt and plate. The velocity profile within the gap was averaged over 200 image pairs and is shown in figure 18. The slight velocity decrease at the top of the gap near the plate indicates that a slight pressure gradient may exist. This profile suggests a lower pressure upstream of the gap.

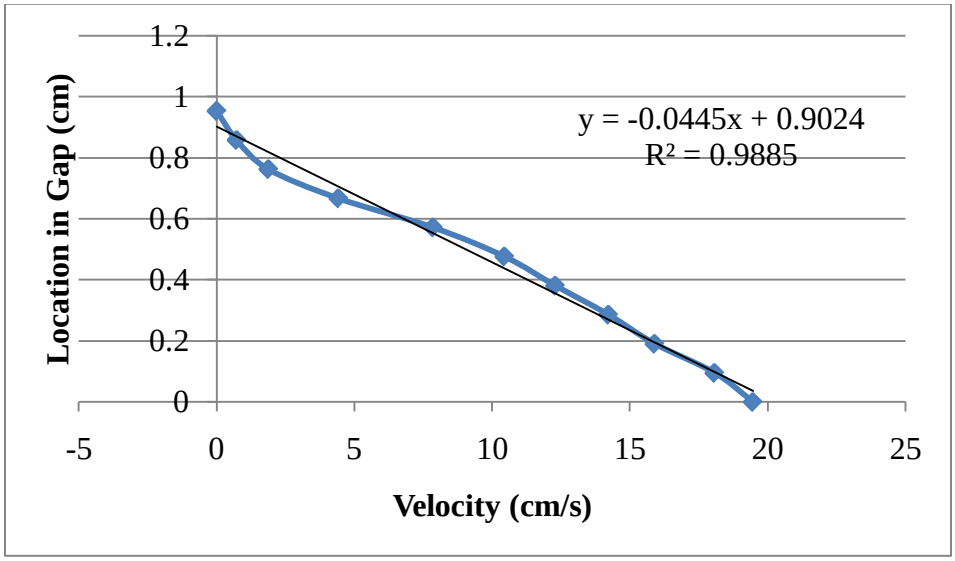

Figure 18. Velocity profile of channel with flat plate.

5.2 Drag Measurements

5.2.1 Flat Plate Model

After the velocity profile was confirmed to be linear, the drag generated by the Couette flow over the flat plate model was measured. Measurements were taken at six different velocities for each of three different gap heights. The gap heights, h, were 0.635 cm (1/4 in), 0.953 cm (3/8 in), and 1.27 cm (1/2 in). The gap heights were non-dimensionalized ($\beta = 2h/l$) by

the cavity length, l = 0.953 cm, which gave three β values of 0.667, 1.00, and 1.33. The velocities at each height were 8.2 cm/s, 15 cm/s, 20 cm/s, 26 cm/s, 32 cm/s, and 38 cm/s. This resulted in Re values tested over a range of 5-50 where near overlap in Re occurred for some of the experiments (i.e. a case with small gap height and higher belt speed had a similar Re to a case with larger gap height and lower belt speed).

The drag measurements were taken over a 10-20 second time span for each velocity and the average was used as the surface drag. This time span was sufficient as equilibrium was achieved after 10 seconds. The graph below shows a drag measurement taken over 100 seconds showing that the average does not change from 10 to 100 seconds. From the data, it was found that the average after 10 seconds was 2.778 N and after 100 seconds it was 2.770 N. The amount was not always decreasing, and no heating occurred with the oil. The temperature of the oil was found to be the same at approximately 22.6°C before and after each experiment.

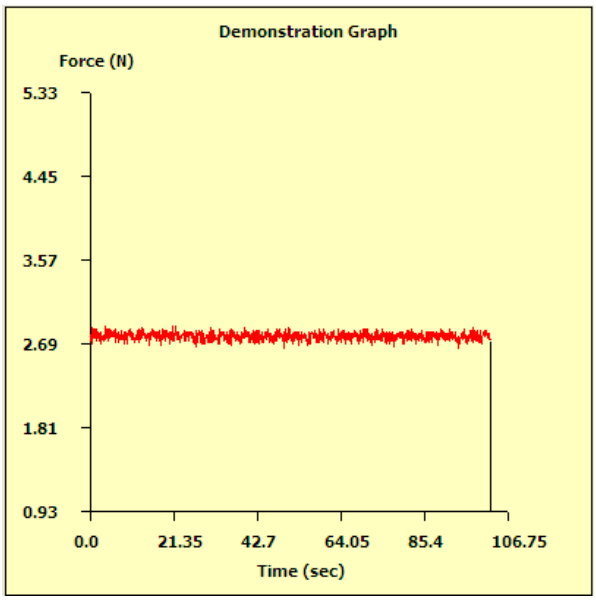

Figure 19. Drag force vs. time over 100 s.

The drag measurements for the two highest velocities at $\beta = 0.667$ could not be taken due to the force being above the 5 N threshold of the force gauge. The measured drag was found to be within 5% or less of the theoretically predicted values. The Reynolds number for the following figure is based on $\gamma_{oil} = 0.86$ and the ρ_{water} at 22.6°C, which was the temperature of the oil during the experiment. The viscosity of the oil was found to be approximately 245 cP ±10 cP (95%). The oil does not have a perfectly uniform viscosity, thus a variation in value was observed over several samples taken; this variation is a result of the production process and was confirmed by the manufacturer. The measured drag force for each belt speed can be seen in figure 19. The data appears to be linear, but when non-dimensionalized all the data falls onto the theoretically predicted drag coefficient versus Re distribution as shown in figure 21.

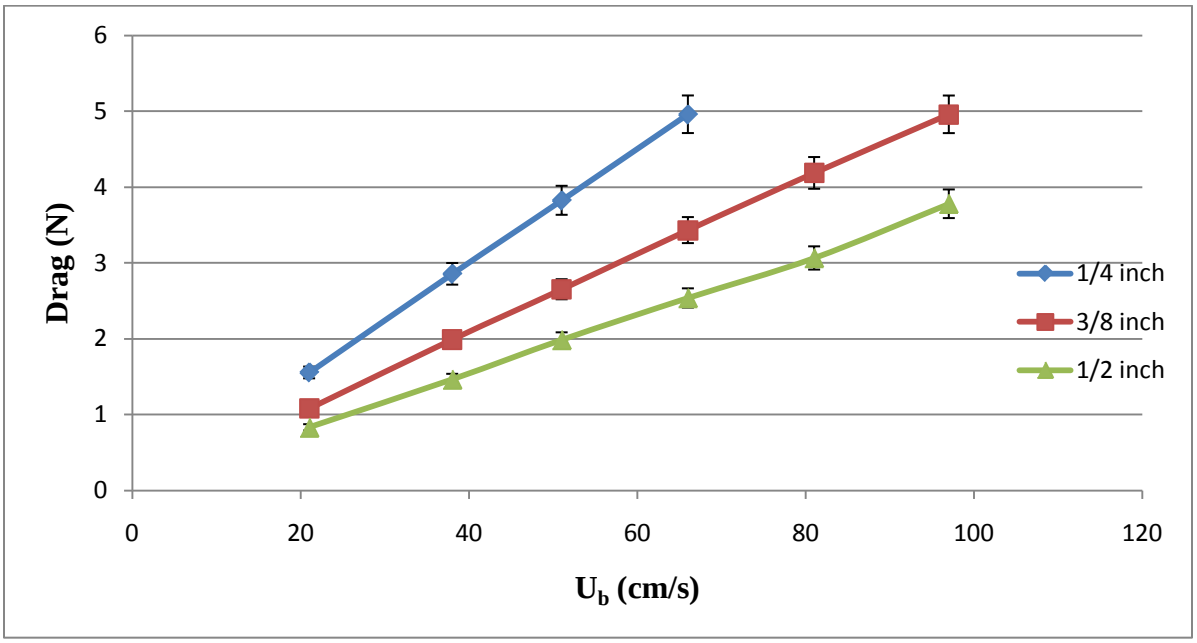

Figure 20. Drag force vs. belt speed for flat plate model.

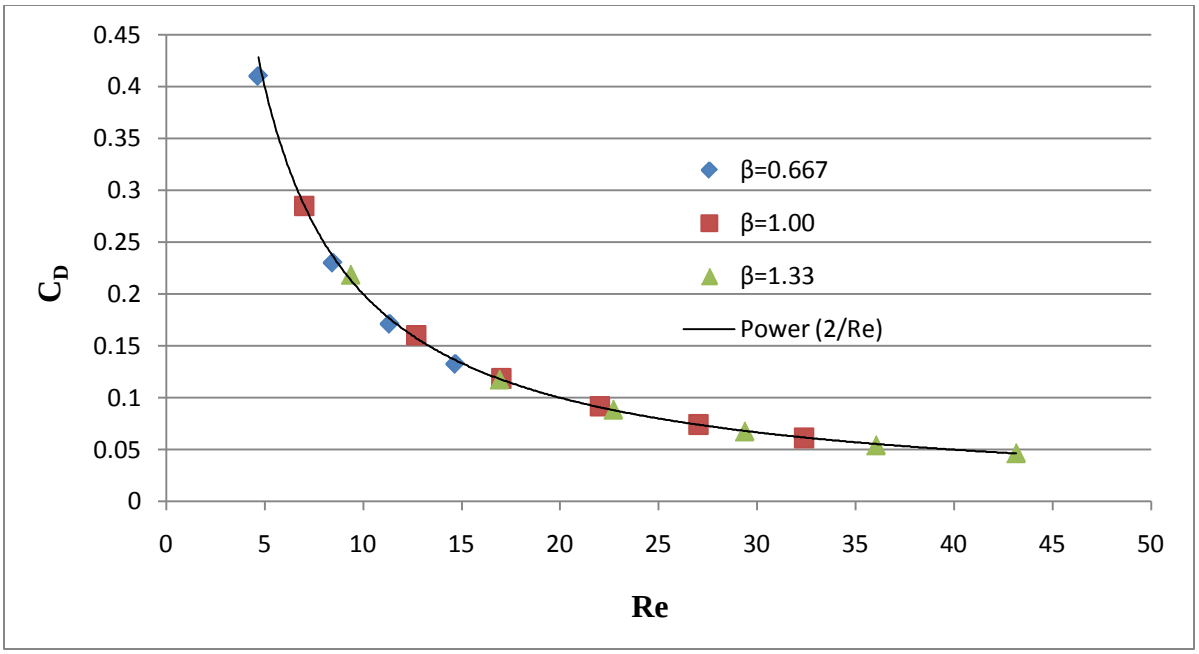

Figure 21. C_D at given Re for flat plate.

In order to compare the difference between the flat plate and the embedded cavity model, only the drag across the area of the cavities was used. The theoretical drag across the edges of the plate where no cavities were present was subtracted from the measured drag. This was done since the measured drag across the flat plate was close to the predicted values as shown in the table below meaning edge effects were minimal. The drag coefficient for the entire flat plate was then determined for each data point and compared to the drag coefficient for just the center area where the cavities were present on the second model. The difference was found to be minimal as shown in figure 21.

β	Belt Velocity (cm/s)	Theoretical Drag (N)	Measured Drag (N)	Drag % Difference
0.667	21	1.622	1.553	-4.241
	38	2.935	2.854	-2.760
	51	3.939	3.824	-2.936
	66	5.098	4.958	-2.738
1	21	1.081	1.079	-0.206
	38	1.956	1.989	1.719
	51	2.625	2.651	0.980
	66	3.397	3.431	0.998
	81	4.169	4.185	0.384
	97	4.992	4.958	-0.697
1.33	21	0.811	0.830	2.300
	38	1.468	1.462	-0.362
	51	1.970	1.983	0.691
	66	2.549	2.536	-0.518
	81	3.128	3.063	-2.078
	97	3.746	3.778	0.847

Table 2. Theoretical and measured drag across a flat plate.

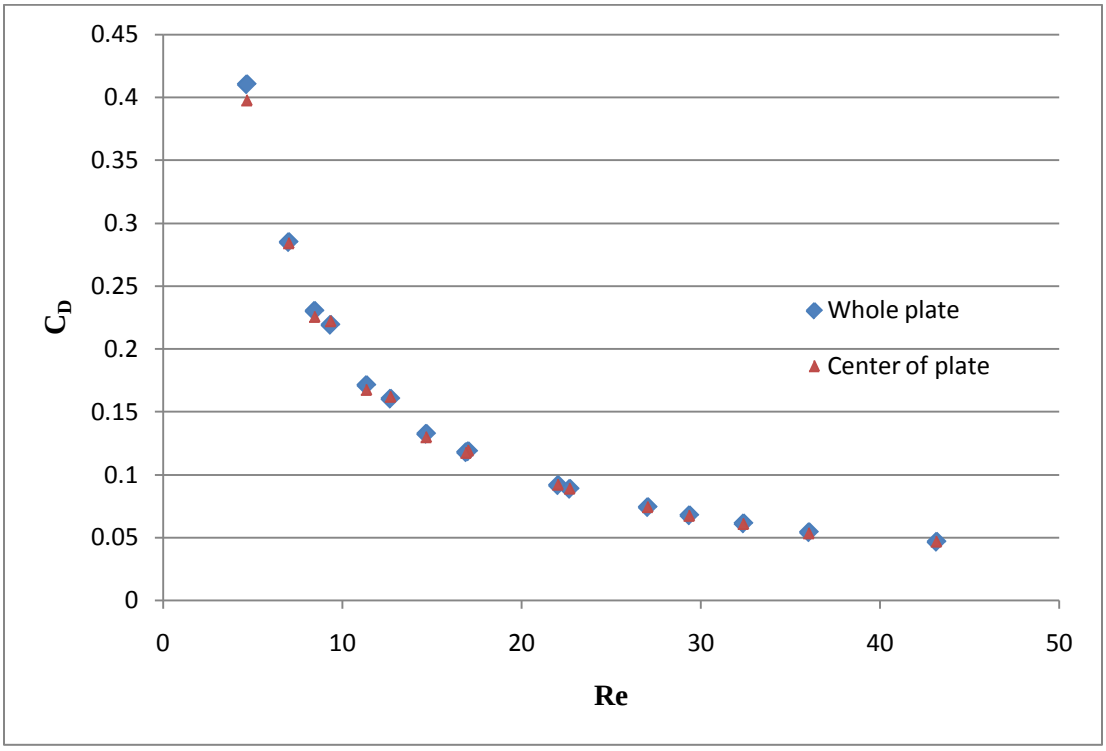

Figure 22. C_D vs. Re for flat plate.

5.2.2 Embedded Cavity Model

The experimental model with the embedded cavities was then placed in the tank and drag measurements across the surface were recorded for the same test parameters as the flat plate. The surface drag across the embedded cavity model was found to be less than that of the flat plate model. Thus the hypothesis, that a low Re regime exists where sub-laminar drag over embedded cavities is realized was experimentally confirmed. The difference was determined to be negligible, (less than 5%) at $\beta = 1.33$. However, for $\beta = 1$ and 0.667 a reduction in the drag coefficient was measured at the lower Re values tested. The drag is shown non-dimensionalized in figure 22.

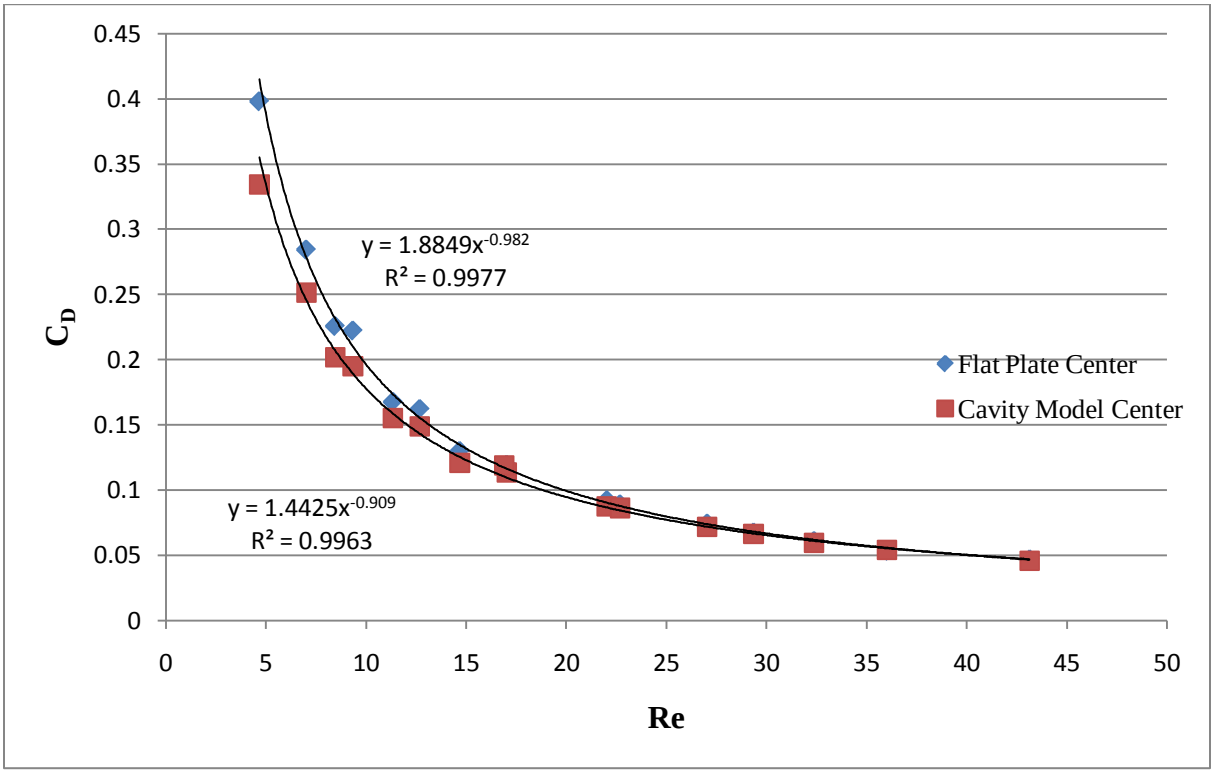

Figure 23. C_D vs. Re for both models.

The C_D percent difference at each Re was found and graphed to see if a relationship existed. Figure 23 shows the relation for each value of β. As can be observed, the data appears to coalesce resulting in significant drag decrease of 10% or more below a Re ~ 10. This result indicates that there is not a significant difference in drag coefficient reduction with the non-dimensional gap height (β). It is interesting to note that the reduction in C_D levels off to a value of around 3% for Re > 30. Gatski and Grosch computationally predicted a value close to this for a single cavity embedded in a boundary layer for over a cavity Re ~ 900.

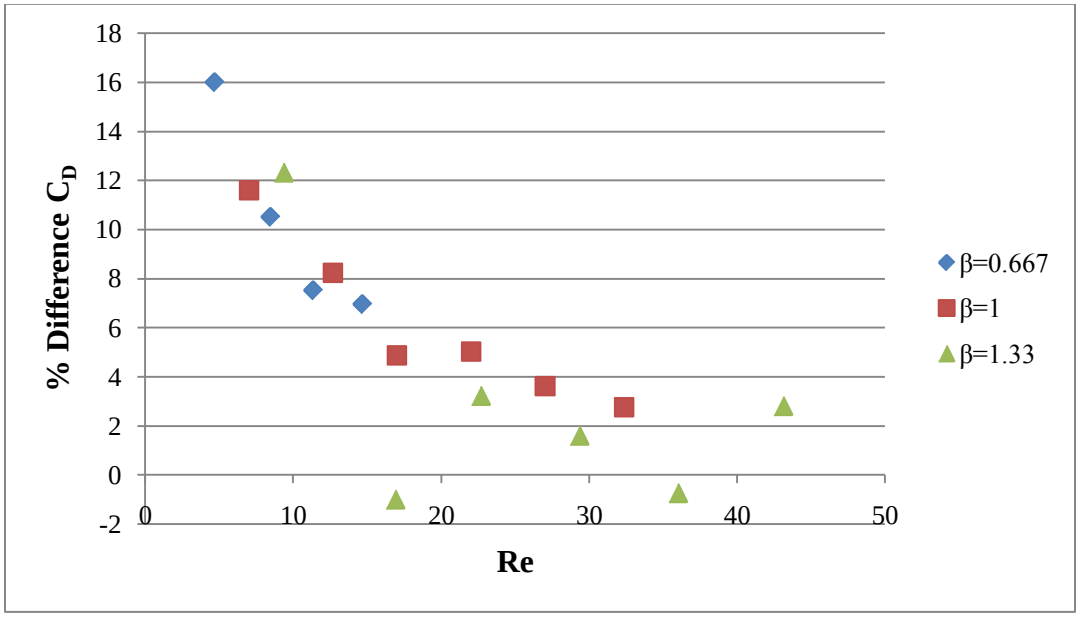

Figure 24. Re vs. % difference C_D for each β value.

The slip velocity could then be found for each trial after the C_D was determined using equation 12. First, the non-dimensional slip velocity is solved using the drag measurements, and then using the belt speed the slip velocity at the top of the embedded cavity surface is calculated. This slip velocity represents an average value for the whole surface; it is theorized that the flow is decelerated to zero at the cavity partitions and proceeds to accelerate across the cavity.

Figures 24 and 25 show Re vs. α and Re vs. u_s for each of the data points in the experiments. There appears to be some dependence in that for smaller gap heights higher slip velocities are achieved. However this difference is not as visible in the previously presented drag reduction data where there appeared to be little dependence on gap height.

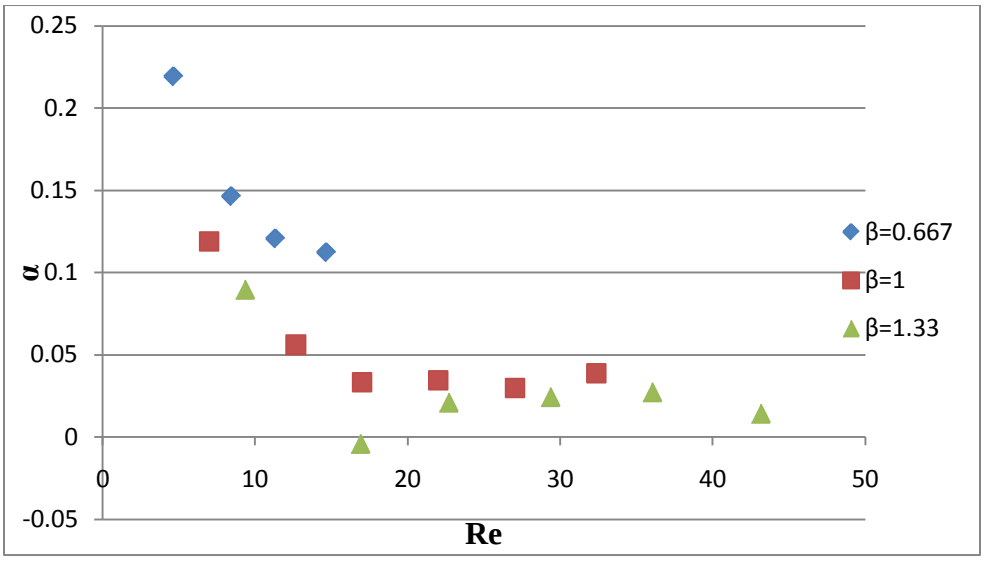

Figure 25. Re vs. α for embedded cavity model.

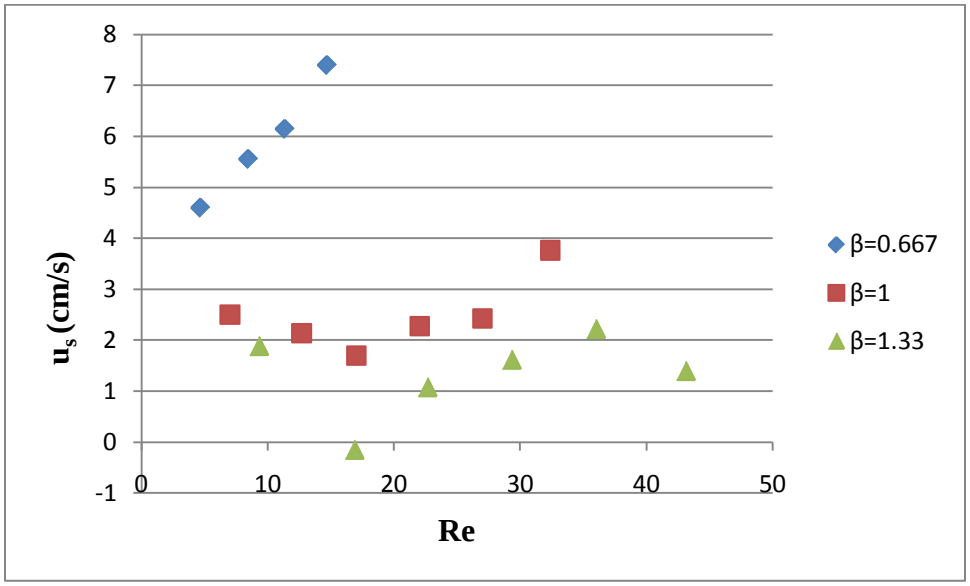

Figure 26. Re vs. u_s for embedded cavity model.

For Re < 15 there appears to be a large increase in α as the Re decreases. The slip velocity seems to be linearly dependent upon the Re for $\beta < 1$. At $\beta > 1$ the slip velocities appeared to remain almost constant and the drag did not seem to be significantly reduced for higher Re values.

6. CONCLUSIONS AND FUTURE WORK

6.1 Couette Flow Facility

The first objective of this research was to build a Couette flow facility. Through PIV measurements it was shown that a linear velocity profile was generated between the moving belt and fixed plate. The flow that resulted was low Reynolds number, well below the transition point since it is known that the embedded cavity geometries would create greater drag than a flat plate in a turbulent flow. The facility is unique in the way that the Couette flow is generated by a conveyor and that low Re drag can be measured across the surface of the fixed plate.

Although the tank itself is relatively small when compared to other oil channels, the wall and edge effects have been proven to be minimal. The flow above the plate has been reduced to almost zero by extending the fixed plate beyond the edge of the moving belt. A slight flow on the surface of the oil may create more drag against the hanging aluminum bars but it is no more than 0.08 N. The mineral oil was chosen because of its high viscosity but the viscosity is not completely constant throughout and was found to vary by ±10 cP.

6.2 Drag Measurements and Partial Slip Velocities

The measured drag values for the flat plate model followed the predicted values for surface drag in a Couette flow. Through this study, it was found that lateral embedded ribs had a surface drag less than that of a flat plate. From the data it was discovered that a low Re regime of sub-laminar drag exists for 2-D embedded cavities. It appears now that this sub-laminar regime exists for $Re < 50$, but this range needs to be investigated further. The drag advantage of

the lateral ribs seems to diminish as the Re increases up to approximately 50 where the drag reduction becomes negligible. The region of higher drag reduction appears to occur for Re < 10 which corresponds with the regime where the drag coefficient begins to dramatically increase as the Re decreases.

Partial slip velocities exist over the embedded cavities as has been shown in previous work. This research provided equations that could be used to back out the average slip velocities within the Couette flow over 2-D embedded cavities.

6.3 Future Work

The Couette flow facility and force measurement apparatus proved to work as planned and predicted. More trials need to be run with varying cavity depth, cavity length, and gap height in order to find the best combination for greatest drag reduction. The aspect ratio of the cavities likely affects the amount of surface drag across the experimental models allowing some width and depth to be the best combination; Wang (1994) predicts greater drag reduction for longer cavities for Re << 1. It is therefore predicted that a greater drag reduction can be achieved likewise in future experiments with Re ~ 1-10 with similar cavity length to depth ratios (l/d) greater than 1. However, a single embedded vortex must be maintained within each cavity which likely will give a maximum l/d between two and three; an increase in drag is predicted when the flow changes such that the outer flow is allowed to move all the way down to the bottom cavities such that positive shear stress occurs at the bottom of the cavities.

More research needs to be done at lower Re, around one or less, to see if the drag reduction levels off and reaches a maximum value at some lower Re above that of the Stokes flow solution analytically predicted by Wang (1994). The extent of the sub-laminar drag regime needs to be investigated to discover future possible drag reduction techniques. The fact that the

drag reduction appeared to be somewhat independent of β is a sign that drag reduction may also be achievable in low Re laminar boundary layer flow, as was indicated as feasible by the computational results of Gatski and Grosch (1985).

Other work may involve using different embedded geometries to find one producing the least amount of drag. Shark skin models used in the University of Alabama water tunnel could be placed in the oil tank and the surface drag can be measured to support water tunnel data. Also, this low Re flow is applicable to the boundary layer flow over butterfly scales with possible application to micro air vehicles. Future work should focus on these areas.

BIBLIOGRAPHY

Ardana, P.H. 2008. "Experimental investigation of the flow over three D-type microgeometries for boundary layer control." PhD diss., University of Alabama.

Aydin, M. & Leutheusser, H.J. 1979. Novel experimental facility for the study of plane Couette flow. *Rev. Sci. Instrum.* **Vol. 50, No. 11,** 1362-1366.

Bakewell, H.P. Jr. 1966. "An experimental investigation of the viscous sublayer in turbulent pipe flow." PhD thesis, Pennsylvania State University.

Bechert, D. W., Bartenwerfer, M., Hoppe, G. & Reif W-E. 1990. Turbulent drag reduction by nonplanar surfaces – a survey on the research at TU/DLR Berlin. *IUTAM Symposium on Structure of Turbulence and Drag Reduction, Zurich 1989.* Springer, Berlin Heidelberg New York.

Bechert, D.W., Hoppe, G., van der Hoeven, J.G.T. & Makris, R. 1992. The Berlin oil channel for drag reduction research. *Experiments in Fluids* **12,** 251-260.

Couette Flow. http://en.wikipedia.org/wiki/Couette_flow. July 2, 2009.

Daviaud, F., Hegseth, J. & Bergé, P. 1992. Subcritical transition to turbulence in plane Couette flow. *Physical Review Letters* **Vol. 69, No. 17,** 2511-2514.

Gatski, T.B., & Grosch, C.E. 1985. Embedded cavity drag in steady laminar flow. *AIAA Journal* **Vol. 23, No. 7,** 1028-1037.

Leutheusser, H.J. & Chu, V.H. 1971. Experiments on plane Couette flow. *Journal of the Hydraulics Division* **9,** 1269-1284.

Melnick, M.B. 2009. "Experimental study of boundary layer flow over three dimensional arrays of embedded cavities." Master's thesis, University of Alabama.

Munson, M. June 20, 2009, personal communication. California Institute of Technology.

Reichardt, H. 1959. Gesetzmaessigkeiten der gradlinigen turbulenten Couettestroemung. *Mitteilungen aus dem Max-Planck-Institut fuer Stroemungsforschung und der Aerodynamischen Versuchsanstalt Goettingen* **No. 22.**

Robertson, J. 1959. On turbulent plane-Couette flow. *Proceedings 6th Annual Conference on Fluid Mechanics* University of Texas, Austin, Texas, 169-182.

Scholle, M., Rund, A. & Aksel, N. 2006. Drag reduction and improvement of material transport in creeping films. *Arch Apple Mech.* **75,** 93-112.

Scholle, M. 2007. Hydrodynamical modeling of lubricant friction between rough surfaces. *Tribology International* **40,** 1004-1011.

Tillmark, N. & Alfredsson, P.H. 1992. Experiments on transition in plane Couette flow. *J. Fluid Mech.* **235,** 89-102.

Wang, C.Y. 1994. The Stokes drag due to the sliding of a smooth plate over a finned plate. *Phys. Fluids* **Vol. 6, No. 7,** 2248-2252.

Watanabe, K., Yanuar, & Udagawa, H. 1999. Drag reduction of Newtonian fluid in a circular pipe with a highly water-repellent wall. *J. Fluid Mech.* **381,** 225-238.

White, F.M. Viscous Fluid Flow. 1991. McGraw-Hill, New York, NY.

APPENDIX 1

According to Wang (1985) an approximately 20% drag reduction can be expected from a square cavity, where a = 0.25 and b = 0.5.

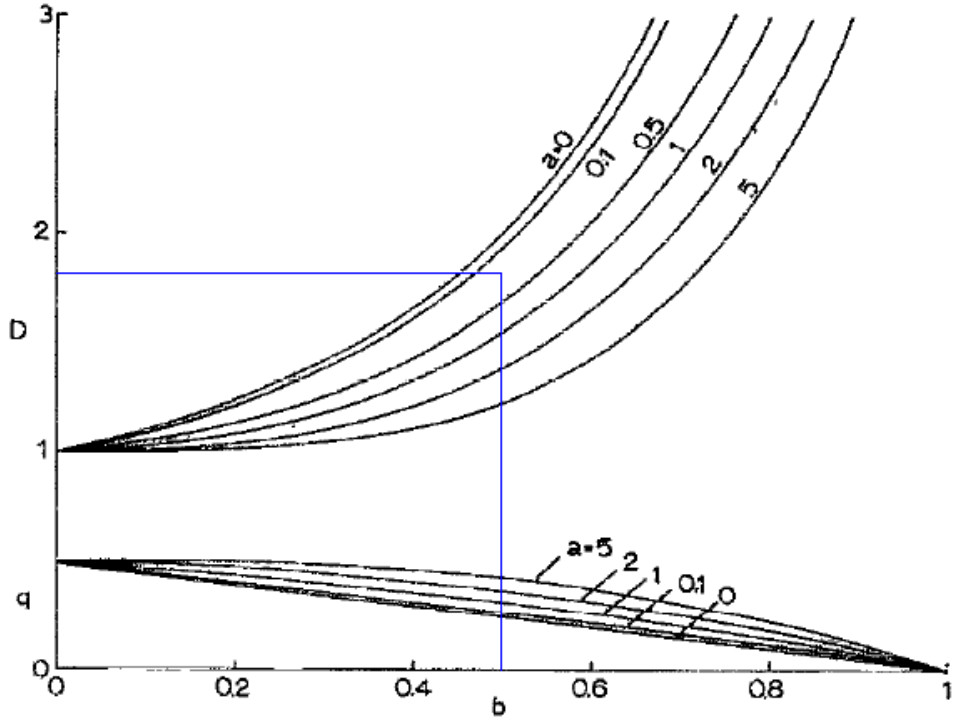

FIG. 5. The drag and flow for the relative motion transverse to the fins.

APPENDIX 2: Lateral Rib Model Drag Measurements

Lateral Rib Model				
Gap Height (cm)	Belt Velocity (cm/s)	2nd Model Measured Drag (N)	Drag over Center Area	% Drag Reduction
0.635	21	1.4085	0.760311024	9.322088457
	38	2.6773	1.504386614	6.19788382
	51	3.6541	2.079926772	4.435494416
	66	4.7546	2.717434646	4.110196838
	81			
	97			
0.953	21	1.0036	0.571700735	6.953458187
	38	1.8899	1.108367996	5.001507992
	51	2.5725	1.523601784	2.946502679
	66	3.3265	1.969102308	3.040107264
	81	4.0939	2.428002833	2.174484456
	97	4.8761	2.881136726	1.643940616
1.27	21	0.7673	0.443205512	7.520790647
	38	1.4711	0.884643307	-0.601791698
	51	1.9447	1.157613386	1.946251197
	66	2.5115	1.492917323	0.958277467
	81	3.0768	1.82672126	-0.440701205
	97	3.7139	2.216892126	1.696664902

APPENDIX 3: Drag Coefficient Data

Results Section Data for Figures							
Re	Cd	Cd center flat plate	Cd center new model	% diff	α	us	2/Re
4.6694	0.4102	0.3981	0.3344	15.9980	0.2193	4.6056	0.4283
8.4494	0.2302	0.2258	0.2021	10.5217	0.1464	5.5614	0.2367
11.3400	0.1712	0.1677	0.1551	7.5394	0.1206	6.1512	0.1764
14.6753	0.1326	0.1301	0.1210	6.9765	0.1122	7.4048	0.1363
7.0078	0.2848	0.2844	0.2514	11.5973	0.1190	2.4992	0.2854
12.6808	0.1604	0.1622	0.1489	8.2377	0.0561	2.1321	0.1577
17.0190	0.1187	0.1194	0.1136	4.8761	0.0332	1.6947	0.1175
22.0246	0.0917	0.0923	0.0877	5.0304	0.0345	2.2778	0.0908
27.0302	0.0743	0.0745	0.0718	3.6125	0.0300	2.4273	0.0740
32.3694	0.0614	0.0611	0.0594	2.7509	0.0388	3.7634	0.0618
9.3389	0.2191	0.2224	0.1949	12.3416	0.0898	1.8866	0.2142
16.8989	0.1179	0.1176	0.1188	-1.0047	-0.0040	-0.1506	0.1184
22.6801	0.0888	0.0892	0.0863	3.2268	0.0211	1.0775	0.0882
29.3507	0.0678	0.0676	0.0665	1.6016	0.0245	1.6173	0.0681
36.0213	0.0544	0.0536	0.0540	-0.7445	0.0274	2.2219	0.0555
43.1366	0.0468	0.0470	0.0457	2.8102	0.0144	1.3956	0.0464